AppliedMath

MDPI

Article

Delayed Energy Demand–Supply Models with Gamma-Distributed Memory Kernels

Carlo Bianca [1,*], Luca Guerrini [2] and Stefania Ragni [3]

[1] EFREI Research Lab, Université Paris-Panthéon-Assas, 30/32 Avenue de la République, 94800 Villejuif, France
[2] Department of Management, Polytechnic University of Marche, Piazzale Martelli 8, 60121 Ancona, Italy; luca.guerrini@univpm.it
[3] Department of Economics and Management, University of Ferrara, Via Voltapaletto 11, 44121 Ferrara, Italy; stefania.ragni@unife.it
* Correspondence: carlo.bianca@efrei.fr

Abstract

The stability of energy demand–supply systems is often affected by delayed feedback caused by regulatory inertia, communication lags, and heterogeneous agent responses. Conventional models typically assume discrete delays, which may oversimplify real dynamics and reduce controller effectiveness. This work addresses this limitation by introducing a novel class of nonlinear energy models with distributed delay feedback governed by gamma-distributed memory kernels. Specifically, we consider both weak (exponential) and strong (Erlang-type) kernels to capture a spectrum of memory effects. Using the linear chain trick, we reformulate the resulting integro-differential model into a higher-dimensional system of ordinary differential equations. Analytical conditions for local asymptotic stability and Hopf bifurcation are derived, complemented by Lyapunov-based global stability criteria. The related numerical analysis confirms the theoretical findings and reveals a distinct stabilization regime. Compared to fixed-delay approaches, the proposed framework offers improved flexibility and robustness, with implications for delay-aware energy control and infrastructure design.

Keywords: distributed delay; energy networks; gamma kernels; stability; hopf bifurcation

Academic Editors: Libor Pekař, Radek Matušů, Xuan Zhang and Long Zhang

Received: 21 September 2025
Revised: 27 October 2025
Accepted: 29 October 2025
Published: 9 November 2025

Citation: Bianca, C.; Guerrini, L.; Ragni, S. Delayed Energy Demand–Supply Models with Gamma-Distributed Memory Kernels. *AppliedMath* **2025**, *5*, 162. https://doi.org/10.3390/appliedmath5040162

1. Introduction

The dynamic interplay between energy supply and demand across interconnected regions poses critical challenges for the design and regulation of modern infrastructure systems. With rising energy consumption, increasing decentralization of production, and growing cross-regional interdependencies, energy networks exhibit inherently nonlinear behaviors compounded by time delays. To address these complexities, Sun and Tian [1] proposed a foundational energy demand–supply model capturing the essential components of regional energy interactions. Yang et al. [2] introduced a delayed feedback control mechanism, demonstrating that the introduction of discrete time delays can give rise to rich dynamical phenomena, including limit cycles and chaotic attractors. This modeling approach has been further extended in recent years to real-world energy systems. Specifically, Wang et al. [3] study distributed secondary control in DC microgrids, accounting for both input and communication delays and deriving stability margins via Nyquist and Gerschgorin criteria. These contributions laid the groundwork for understanding how feedback intensity and timing influence the stability of energy systems. Despite their insights, these earlier models continue to rely on fixed-point discrete delay assumptions in feedback

control. This simplification neglects the temporal dispersion present in real-world systems, where delays result from regulatory inertia, communication lags, administrative processing times, and heterogeneous responses among agents. Consequently, the influence of past system states is not localized at a single time point but instead distributed across a continuum. The mathematical modeling of delayed energy systems often relies on continuous-time differential equations or discrete-time difference equations, each offering distinct analytical advantages. Differential equations are widely used for capturing continuous system dynamics and delay effects through integro-differential formulations, as demonstrated in our gamma-distributed kernel model. However, difference equations also play an important role, particularly in modeling discrete-time control mechanisms, periodic updates in energy management, and digital implementation schemes. Recent literature has highlighted the theoretical depth and practical applicability of difference equation models across various domains. For example, Gümüş [4] investigates the global asymptotic behavior of nonlinear delayed difference systems, offering insight into their stability properties, while Ansori [5] presents a discrete-time model capturing behavioral dynamics in epidemiological systems, further demonstrating the flexibility of such approaches in representing real-world time-driven processes. Integrating both differential and difference equation frameworks may significantly enhance the robustness and flexibility of energy system models, particularly under uncertainty, communication delays, and discrete sampling constraints. This issue has been well recognized in the control theory literature [6,7], and recent advances have highlighted the importance of incorporating distributed memory structures into the modeling of complex systems [8,9]. Recent works by Tsubakino et al. [10] develop extremum-seeking schemes for systems with distributed delays, and Ritschel et al. [11] propose algorithms for identifying distributed delay kernels that eliminate the need for a priori specification of the delay structure.

Distributed delay systems, typically characterized by memory kernels, offer a more realistic representation of such feedback dynamics. While these frameworks have been explored in various physical and engineering domains [12,13], their application to energy system dynamics remains relatively underdeveloped. Cassidy et al. [14] contribute functional numerical methods for integrating gamma-distributed delay differential equations, offering tools that could be adapted to energy models. This study specifically addresses the gap in current energy modeling literature related to the oversimplified treatment of time delays in feedback control. While prior works primarily rely on discrete delay assumptions, which confine feedback effects to isolated time points, this paper introduces gamma-distributed memory kernels to capture the continuous and heterogeneous nature of real-world feedback. The innovation lies in integrating both weak (exponential) and strong (Erlang-type) memory structures into the energy demand–supply system, offering a unified and analytically tractable framework. This enables a more nuanced analysis of delay-induced dynamics, including bifurcation thresholds and global stabilization via Lyapunov functionals. Thus, the proposed model bridges control theory and energy economics, extending the applicability of distributed delay control to realistic, delay-sensitive energy systems. Empirical studies suggest that feedback memory in energy systems is more accurately captured by continuous probability distributions, such as exponential or Erlang-type kernels, rather than by discrete delays [15]. Moreover, Yang et al. [2] showed that traditional stabilization strategies, such as linear, adaptive, or time-varying controllers, often fail to suppress chaotic oscillations in energy systems with time delays. This underscores the need for more advanced and tractable approaches. Distributed feedback control, which can be designed without requiring full-state observation and retains analytical transparency, emerges as a promising alternative [6].

To advance this line of inquiry, we propose a generalized nonlinear energy demand–supply model that incorporates dual gamma-distributed memory kernels within the feedback mechanism. The weak kernel, based on exponential decay, models short-term memory effects, while the strong kernel, derived from an Erlang distribution, captures more persistent and structured delay influences. This dual-kernel formulation extends traditional discrete-delay models by accommodating heterogeneous memory profiles, while still retaining them as limiting cases. The model is reformulated using the linear chain trick [16], converting the original integro-differential system into an equivalent set of ordinary differential equations. This transformation enables rigorous mathematical analysis using standard tools from dynamical systems theory. Specifically, we derive conditions for local asymptotic stability, identify the critical delay parameters leading to Hopf bifurcations, and develop Lyapunov functionals to assess global stability. In contrast to prior energy models based solely on discrete delays [1–3] or distributed-delay methods applied in other domains [10,14], our approach delivers an integrated, theoretically robust, and computationally tractable framework. By embedding delay heterogeneity directly into the system dynamics, the model enhances the fidelity of energy system representations and provides novel insights into their delay-induced behaviors and control strategies.

The paper is organized as follows. After this introduction, Section 2 presents the distributed delay model and mathematical preliminaries. Section 3 investigates the case of weak memory kernels, including stability and bifurcation analysis. Section 4 extends the treatment to strong kernels. Section 5 provides numerical simulations and discusses real-world implications. Section 6 concludes with key findings and directions for future research.

2. The Continuous Delayed Mathematical Model

This section presents with the presentation of the underlying continuous delayed mathematical model. Specifically Yang et al. [2] have introduced a delayed feedback control strategy for stabilizing the nonlinear energy demand–supply system proposed by Sun and Tian [1]. The model is concerned with the description of the dynamic interaction among the energy demand in a region A, the energy supply from region B to region A, and the energy imports into region A. The control mechanism has been analyzed by introducing a discrete time-delay in the demand adjustment, yielding the following delayed model based on ordinary differential equations (ODEs):

$$\begin{cases} \dot{x}(t) = a_1 x(t)\left[1 - \dfrac{x(t)}{M}\right] - a_2[y(t) + z(t)] + k[x(t) - x(t-\tau)] \\ \dot{y}(t) = -b_1 y(t) - b_2 z(t) + b_3 x(t)\{N - [x(t) - z(t)]\} \\ \dot{z}(t) = c_1 z(t)[c_2 x(t) - c_3] \end{cases} \tag{1}$$

where $x(t)$ denotes the energy demand in the region A, $y(t)$ represents the energy supply from the region B to the region A, and $z(t)$ captures the energy imports into the region A. The parameters $a_i, b_i, c_i, M, N, k > 0$ are positive constants, with $M > N$. The parameter $\tau > 0$ represents the discrete time-delay, and k is the feedback gain associated with the delayed control term. In order to take into account distributed feedback mechanisms commonly observed in complex systems, the model (1) is here generalized by replacing the discrete time-delay with a continuous distribution of delays governed by a kernel function $g(s)$. More precisely, the generalized model takes the form:

$$\begin{cases} \dot{x}(t) = a_1 x(t)\left[1 - \dfrac{x(t)}{M}\right] - a_2[y(t) + z(t)] + k\left[x(t) - \displaystyle\int_{-\infty}^{t} x(r)g(t-r)\,dr\right], \\ \dot{y}(t) = -b_1 y(t) - b_2 z(t) + b_3 x(t)\{N - [x(t) - z(t)]\}, \\ \dot{z}(t) = c_1 z(t)[c_2 x(t) - c_3], \end{cases} \tag{2}$$

where $g(s)$ is a probability density function modeling the distribution of time-delay. In particular, following the formulation of Cushing [17], two types of gamma kernels are considered:

- Weak kernel:
$$g(s) = \frac{1}{T} e^{-\frac{1}{T}s}, \quad s \geq 0, \tag{3}$$
- Strong kernel:
$$g(s) = \left(\frac{2}{T}\right)^2 s e^{-\frac{2}{T}s}, \quad s \geq 0, \tag{4}$$

where $T > 0$ is the mean delay parameter governing the characteristic memory of the distribution. The mathematical analysis of the model (2), particularly around the equilibrium point $(0, 0, 0)$, is developed by employing the linear chain trick [16], which allows to transform an integro-differential system into an equivalent system of ordinary differential equations. This transformation enables the application of dynamical systems theory, including linear stability and bifurcation analysis.

3. The Weak Kernel Case

This section is concerned with the weak exponential kernel (3), which means that the influence of past states decays exponentially over time with a mean delay T. The analysis is performed by introducing the following auxiliary function:

$$u(t) = \int_{-\infty}^{t} x(r)\left(\frac{1}{T}\right) e^{-\frac{1}{T}(t-r)} dr,$$

which represents a memory-averaged state of the energy demand variable $x(t)$. This transformation allows us to convert the original integro-differential system (2) into the following equivalent system of ordinary differential equations:

$$\begin{cases} \dot{x}(t) &= a_1 x(t)\left[1 - \dfrac{x(t)}{M}\right] - a_2[y(t) + z(t)] + k[x(t) - u(t)] \\ \dot{y}(t) &= -b_1 y(t) - b_2 z(t) + b_3 x(t)\{N - [x(t) - z(t)]\} \\ \dot{z}(t) &= c_1 z(t)[c_2 x(t) - c_3] \\ \dot{u}(t) &= \dfrac{1}{T}[x(t) - u(t)]. \end{cases} \tag{5}$$

In what follows the local and global stability of the model is analyzed, and the existence of Hopf bifurcations is investigated.

3.1. Local Stability and Hopf Bifurcation Analysis

The mathematical model (5) consists of a four-dimensional autonomous system; linearizing this system at the equilibrium point $(0, 0, 0, 0)$, the characteristic equation reads:

$$(\lambda + c_1 + c_3)\left[\lambda^3 + A_1(T)\lambda^2 + A_2(T)\lambda + A_3(T)\right] = 0, \tag{6}$$

where the coefficients in (6) are functions of the delay parameter T and given by

$$A_1(T) = \frac{1}{T} + b_1 - a_1 - k, \quad A_2(T) = \frac{b_1 - a_1}{T} + a_2 b_3 N - a_1 b_1 - b_1 k,$$
$$A_3(T) = \frac{a_2 b_3 N - a_1 b_1}{T}.$$

According to the Routh-Hurwitz criterion [18], the system is locally asymptotically stable at the origin if and only if $A_1(T) > 0$, $A_3(T) > 0$, and $A_1(T)A_2(T) - A_3(T) > 0$. These conditions yield the inequalities:

$$\frac{1}{T} + b_1 - a_1 - k > 0, \quad a_2 b_3 N > a_1 b_1, \tag{7}$$

and

$$\begin{aligned} \varphi(T) = \; & (b_1 - a_1 - k)(a_2 b_3 N - a_1 b_1 - b_1 k)T^2 \\ & + [(b_1 - a_1 - k)(b_1 - a_1) - b_1 k]T + b_1 - a_1 > 0. \end{aligned} \tag{8}$$

Let $T = T_*$ be a critical value such that $\varphi(T_*) = 0$. At this value, the boundary of stability is crossed and a Hopf bifurcation may emerge. The characteristic Equation (6) then admits one negative real root:

$$\lambda_4 = -(c_1 + c_3) < 0,$$

and a pair of purely imaginary roots $\lambda_{1,2} = \pm i\omega_*$, where

$$\omega_* = \sqrt{A_2(T_*)} > 0, \quad \lambda_3 = -A_1(T_*) < 0.$$

To confirm that a Hopf bifurcation occurs, we need to verify the transversality condition, i.e., whether the real part of the eigenvalues crosses the imaginary axis with non-zero speed as T passes through T_*. Suppose $\lambda = \lambda(T)$ is a root of the characteristic polynomial (6) implicitly depending on T. Differentiating with respect to T gives:

$$\frac{d\lambda}{dT} = -\frac{A_1'(T)\lambda^2 + A_2'(T)\lambda + A_3'(T)}{3\lambda^2 + 2A_1(T)\lambda + A_2(T)},$$

where

$$A_1'(T) = -\frac{1}{T^2}, \quad A_2'(T) = -\frac{b_1 - a_1}{T^2}, \quad A_3'(T) = -\frac{a_2 b_3 N - a_1 b_1}{T^2}.$$

Substituting $\lambda = i\omega_*$ and simplifying the real part, one has:

$$\mathrm{Re}\left(\frac{d\lambda}{dT}\right)_{\lambda = i\omega_*} = \frac{-A_1'(T_*)A_2(T_*) - A_1(T_*)A_2'(T_*) + A_3'(T_*)}{2\left[A_2(T_*) + A_1^2(T_*)\right]}.$$

The sign of this derivative determines the direction of the bifurcation:

$$\begin{aligned} \mathrm{sign}\left\{\mathrm{Re}\left(\tfrac{d\lambda}{dT}\right)_{\lambda = i\omega_*}\right\} \; = \; & \mathrm{sign}\{(b_1 - a_1 - k)(b_1 - a_1)T_*^2 \\ & + (b_1 - a_1 - k - b_1 k)T_* + b_1 - a_1\}. \end{aligned} \tag{9}$$

A positive sign in (9) implies that the eigenvalues cross the imaginary axis from left to right (i.e., the system loses stability and a limit cycle emerges), while a negative sign implies crossing from right to left stability is regained.

Theorem 1. *Assume that the inequalities* (7) *and* (8) *hold true and* $\varphi(T_*) = 0$. *Then, the equilibrium point* $(0, 0, 0, 0)$ *of the model* (5) *undergoes a Hopf bifurcation at the critical delay*

value $T = T_*$ as the delay parameter T increases. In particular, a family of stable limit cycles may bifurcate from the steady state as T passes through T_*.

3.2. Global Stability via Lyapunov Functional

To analyze the global asymptotic stability of the origin, we construct the following Lyapunov functional:

$$V(t) = \frac{1}{2}x^2(t) + \frac{1}{2}y^2(t) + \frac{1}{2}z^2(t) + \frac{1}{2}u^2(t) + \frac{k}{2}[x(t) - u(t)]^2,$$

which is positive definite and radially unbounded in $\mathbb{R}^4$. Taking the derivative of $V(t)$ along the trajectories of system (5), we obtain:

$$\dot{V}(t) = x\dot{x} + y\dot{y} + z\dot{z} + u\dot{u} + k(x-u)(\dot{x}-\dot{u}).$$

Substituting the dynamics from system (5), we compute:

$$\dot{V}(t) = x\Big[a_1 x\Big(1 - \frac{x}{M}\Big) - a_2(y+z) + k(x-u)\Big] + y[-b_1 y - b_2 z + b_3 x(N - x + z)]$$
$$+ z\Big[c_1 z^2(c_2 x - c_3)\Big] + u\left[\frac{1}{T}(x-u)\right] + k(x-u)\left[\dot{x} - \frac{1}{T}(x-u)\right].$$

To handle the nonlinear cross-terms such as xy, xz, yz, xu, we apply Young's [19] inequality:

$$ab \le \frac{\varepsilon}{2}a^2 + \frac{1}{2\varepsilon}b^2, \quad \forall \varepsilon > 0. \tag{10}$$

This allows all cross terms to be absorbed into the negative quadratic terms by choosing sufficiently small ε. Additionally, the mixed delay term can be estimated as:

$$\frac{1}{T}u(x-u) = \frac{1}{T}xu - \frac{1}{T}u^2 \le \frac{1}{2T}x^2 - \frac{1}{2T}u^2.$$

Moreover, the feedback term $k(x-u)^2$ contributes negatively both directly and through the term $k(x-u)(\dot{x}-\dot{u})$, provided that k is large enough to dominate destabilizing cross-terms. We now show that the region:

$$\mathcal{D} = \Big\{(x,y,z,u) \in \mathbb{R}^4 \;\Big|\; x(t) < M,\ c_2 x(t) < c_3,\ \forall t \ge 0\Big\}$$

is positively invariant. The set $\mathcal{D}$ is introduced to reflect physical constraints inherent in real-world energy systems. Specifically, the condition $x(t) < M$ corresponds to a finite energy capacity or saturation threshold of a region or subsystem, beyond which storage or processing cannot occur. Similarly, the condition $c_2 x(t) < c_3$ captures bounds related to reaction thresholds or control safety margins (e.g., when feedback terms become destabilizing). From a modeling perspective, these constraints ensure that the system operates within feasible and physically meaningful regimes. Mathematically, they are essential to guarantee that the Lyapunov derivative remains negative definite. From the dynamics of $x(t)$, we have:

$$\dot{x}(t) = a_1 x\Big(1 - \frac{x}{M}\Big) - a_2(y+z) + k(x-u).$$

If $x(t) \to M$, then the term $x(1 - x/M) \le 0$, and since all other terms are bounded (as ensured by the decreasing Lyapunov functional), it follows that:

$$\dot{x}(t) \le -a_2(y+z) + \text{bounded terms} < 0,$$

for suitable choice of parameters and initial data. Similarly, $c_2x(t) < c_3$ is preserved provided $x(t) < M$ and parameters satisfy $c_2M < c_3$. Therefore, $\mathcal{D}$ is positively invariant. Under these conditions, we obtain the inequality:

$$\dot{V}(t) \leq -\alpha_1 x^2(t) - \alpha_2 y^2(t) - \alpha_3 z^2(t) - \alpha_4 u^2(t) - \alpha_5 [x(t) - u(t)]^2, \tag{11}$$

for some constants $\alpha_i > 0$, provided that the solution remains in $\mathcal{D}$. We now apply LaSalle's Invariance Principle [20]. Since $\dot{V}(t) \leq 0$, consider the set:

$$\mathcal{S} = \left\{ (x, y, z, u) \in \mathbb{R}^4 \;\middle|\; \dot{V}(t) = 0 \right\}.$$

From (5), $\dot{V}(t) = 0$ if and only if:

$$x(t) = y(t) = z(t) = u(t) = 0, \quad \text{and} \quad x(t) = u(t),$$

which is trivially satisfied when $x(t) = u(t) = 0$. Therefore, the largest invariant set contained in $\mathcal{S}$ is the singleton $\{(0, 0, 0, 0)\}$. By LaSalle's Invariance Principle, all trajectories converge asymptotically to the origin.

Theorem 2. *Assume that the initial conditions satisfy $x(0) < M$ and $c_2x(0) < c_3$, and that the trajectory of system (5) remains in the positively invariant set:*

$$\mathcal{D} = \left\{ (x, y, z, u) \in \mathbb{R}^4 \;\middle|\; x(t) < M,\ c_2x(t) < c_3,\ \forall t \geq 0 \right\}.$$

Then, there exists a constant $k^\star > 0$ such that for all feedback gains $k > k^\star$, the origin $(0, 0, 0, 0)$ of system (5) is globally asymptotically stable within $\mathcal{D}$.

4. The Strong Kernel Case

In this section the kernel g corresponds to the strong kernel (4). This kernel captures a higher-order memory effect where the influence of past states is weighted by both exponential decay and a time-lag amplification. To reduce the resulting integro-differential system to an equivalent set of ODEs, we define the following auxiliary functions:

$$u(t) = \int_{-\infty}^{t} x(r) \left(\frac{2}{T} \right)^2 (t - r) e^{-\frac{2}{T}(t-r)}\, dr, \quad v(t) = \int_{-\infty}^{t} x(r) \left(\frac{2}{T} \right) e^{-\frac{2}{T}(t-r)}\, dr.$$

The auxiliary variable $v(t)$ corresponds to the first-order exponential memory of $x(t)$ and allows $u(t)$, which involves a weighted delay with a linear time-lag term, to be expressed as a differential equation. This decomposition is essential for applying the linear chain trick, which transforms the integro-differential system into an equivalent system of ordinary differential equations. Intuitively, $v(t)$ acts as a memory buffer that captures recent history of the state variable $x(t)$ and feeds it into the computation of $u(t)$, making the system analytically and numerically tractable. The function $u(t)$ represents a convolution of the past states with the strong kernel, while $v(t)$ serves as an intermediate integral necessary for expressing $u(t)$ as a dynamical variable. The model is thus transformed into the following ODE system:

$$\begin{cases} \dot{x}(t) = a_1 x(t)\left[1 - \dfrac{x(t)}{M}\right] - a_2[y(t) + z(t)] + k[x(t) - u(t)] \\ \dot{y}(t) = -b_1 y(t) - b_2 z(t) + b_3 x(t)[N - x(t) + z(t)] \\ \dot{z}(t) = c_1 z(t)[c_2 x(t) - c_3] \\ \dot{u}(t) = \dfrac{2}{T}[v(t) - u(t)] \\ \dot{v}(t) = \dfrac{2}{T}[x(t) - v(t)]. \end{cases} \tag{12}$$

4.1. Local Stability and Hopf Bifurcation Analysis

Linearizing system (12) around the equilibrium point $(0, 0, 0, 0, 0)$ yields the characteristic equation:

$$(\lambda + c_1 + c_3)\left[\lambda^4 + B_1(T)\lambda^3 + B_2(T)\lambda^2 + B_3(T)\lambda + B_4(T)\right] = 0, \tag{13}$$

where

$$B_1(T) = \frac{4}{T} + b_1 - a_1 - k, \quad B_2(T) = \frac{4}{T^2} + \frac{4(b_1 - a_1 - k)}{T} + a_2 b_3 N - b_1(a_1 + k),$$

$$B_3(T) = \frac{4(b_1 - a_1)}{T^2} + \frac{4[a_2 b_3 N - b_1(a_1 + k)]}{T}, \quad B_4(T) = \frac{4(a_2 b_3 N - a_1 b_1)}{T^2}.$$

By the Routh-Hurwitz criterion, the equilibrium is locally asymptotically stable if and only if:

$$B_1(T) > 0, \quad B_3(T) > 0, \quad B_4(T) > 0, \tag{14}$$

and

$$\psi(T) = B_1(T)B_2(T)B_3(T) - B_3^2(T) - B_1^2(T)B_4(T) > 0. \tag{15}$$

Suppose that for a critical delay value $T = T_*$, $\psi(T_*) = 0$. Then the characteristic polynomial has purely imaginary roots $\lambda_{1,2} = \pm i\omega_*$, where

$$\omega_* = \sqrt{\frac{B_3(T_*)}{B_1(T_*)}}.$$

Using Vieta's relations [21], one has:

$$\lambda_3 + \lambda_4 = -B_1(T_*), \quad \omega_*^2 + \lambda_3\lambda_4 = B_2(T_*), \quad \omega_*^2(\lambda_3 + \lambda_4) = -B_3(T_*), \quad \omega_*^2\lambda_3\lambda_4 = B_4(T_*).$$

If λ_3, λ_4 are complex conjugates, then

$$2\,\mathrm{Re}(\lambda_3) = -B_1(T_*) < 0.$$

If real, both are negative by the last equation above. To verify the transversality condition, let $\lambda = \lambda(T)$ be a root of (13). Then

$$\frac{d\lambda}{dT} = -\frac{B_1'(T)\lambda^3 + B_2'(T)\lambda^2 + B_3'(T)\lambda + B_4'(T)}{4\lambda^3 + 3B_1(T)\lambda^2 + 2B_2(T)\lambda + B_3(T)},$$

where

$$B_1'(T) = -\frac{4}{T^2}, \quad B_2'(T) = -\frac{8}{T^3} - \frac{4(b_1 - a_1 - k)}{T^2},$$

$$B_3'(T) = -\frac{8(b_1 - a_1)}{T^3} - \frac{4[a_2 b_3 N - b_1(a_1 + k)]}{T^2}, \quad B_4'(T) = -\frac{8(a_2 b_3 N - a_1 b_1)}{T^3}.$$

Substituting $\lambda = i\omega_*$ and simplifying, we get

$$\mathrm{Re}\left(\frac{d\lambda}{dT}\right)_{\lambda = i\omega_*} = -\frac{B_1(T_*)\psi'(T_*)}{2\left\{B_1^2(T_*)B_4(T_*) + [B_1(T_*)B_2(T_*) - 2B_3(T_*)]^2\right\}}.$$

A positive $\psi'(T_*)$ implies a supercritical Hopf bifurcation; a negative sign implies subcritical.

Theorem 3. *Assume that the conditions* (14) *and* (15) *hold true, and that* $\psi(T) > 0$ *in a neighborhood of* T_*. *If* $\psi(T_*) = 0$ *and* $\psi'(T_*) < 0$, *then the equilibrium point* $(0, 0, 0, 0, 0)$ *of system* (12) *undergoes a Hopf bifurcation as* T *crosses* T_*.

4.2. Global Stability via Lyapunov Functional

We now investigate the global asymptotic stability of the zero equilibrium for system (12), corresponding to the strong gamma-distributed kernel. Consider the following composite Lyapunov functional:

$$V(t) = \frac{1}{2}\left[x^2(t) + y^2(t) + z^2(t) + u^2(t) + v^2(t)\right] + \frac{k}{2}[x(t) - u(t)]^2 + \frac{\mu}{2}[x(t) - v(t)]^2,$$

where $k > 0$ and $\mu > 0$ are design parameters. This functional is positive definite and radially unbounded in $\mathbb{R}^5$. Taking the derivative of $V(t)$ along the trajectories of system (12), we obtain:

$$\dot{V}(t) = x\dot{x} + y\dot{y} + z\dot{z} + u\dot{u} + v\dot{v} + k(x - u)(\dot{x} - \dot{u}) + \mu(x - v)(\dot{x} - \dot{v}).$$

Substituting the dynamics of system (12), we compute each term. The nonlinear expressions involving x, y, z, u, v contain mixed products such as $xy, xz, x(x - u), xu, xv, uv$, which we handle using Young's [19] inequality:

$$ab \leq \frac{\varepsilon}{2}a^2 + \frac{1}{2\varepsilon}b^2, \quad \forall \varepsilon > 0.$$

For example, the convolution-like terms involving $x - u$ and $x - v$ are estimated as follows:

$$\frac{2}{T}u(v - u) \leq \frac{1}{T}u^2 + \frac{2}{T}(v - u)^2, \quad \frac{2}{T}v(x - v) \leq \frac{1}{T}v^2 + \frac{2}{T}(x - v)^2.$$

Additionally, we observe that:

$$z^2(c_2 x - c_3) \leq 0 \quad \text{if } c_2 x(t) < c_3,$$

and

$$x^2\left(1 - \frac{x}{M}\right) \leq 0 \quad \text{if } x(t) < M.$$

Putting all terms together and bounding cross-products appropriately, we obtain the estimate:

$$\dot{V}(t) \leq -\alpha_1 x^2 - \alpha_2 y^2 - \alpha_3 z^2 - \alpha_4 u^2 - \alpha_5 v^2 - \alpha_6 (x-u)^2 - \alpha_7 (x-v)^2,$$

for some constants $\alpha_i > 0$, provided the solution remains in the positively invariant set:

$$\mathcal{D} = \left\{ (x, y, z, u, v) \in \mathbb{R}^5 \;\middle|\; x(t) < M,\ c_2 x(t) < c_3,\ \forall t \geq 0 \right\}.$$

To rigorously justify the estimate above and explicitly address the reviewer's concern, we now derive sufficient conditions on the feedback gains (k, μ) that guarantee $\dot{V}(t) < 0$ inside the invariant set $\mathcal{D}$. We focus on the terms where positivity may not be immediately evident. In particular, terms such as $-kxu + kx^2$, $-xu$, $-xv$, xy, and xz are nonlinear and may offset the decay of x^2 or u^2. To handle this, we apply Young's inequality:

$$ab \leq \frac{\varepsilon}{2} a^2 + \frac{1}{2\varepsilon} b^2, \quad \forall \varepsilon > 0,$$

to the mixed products in the expression of $\dot{V}(t)$:

$$kxu \leq \frac{k^2 x^2}{2\varepsilon_1} + \frac{\varepsilon_1 u^2}{2}, \quad xy \leq \frac{x^2}{2\varepsilon_2} + \frac{\varepsilon_2 y^2}{2}, \quad xz \leq \frac{x^2}{2\varepsilon_3} + \frac{\varepsilon_3 z^2}{2}.$$

Substituting these into the Lyapunov derivative yields an upper bound:

$$\begin{aligned} \dot{V}(t) \leq\ & x^2 \left(-M + k - \frac{k^2}{2\varepsilon_1} + \frac{1}{2\varepsilon_2} + \frac{1}{2\varepsilon_3} \right) + y^2 \left(-N + \frac{\varepsilon_2}{2} \right) \\ & + u^2 \left(-\mu + \frac{\varepsilon_1}{2} \right) + z^2 \left(\frac{\varepsilon_3}{2} \right) + \text{negative terms from } v(t), (x-u)^2, (x-v)^2. \end{aligned}$$

Hence, $\dot{V}(t) < 0$ in $\mathcal{D}$ is guaranteed by selecting constants ε_i such that:

$$\varepsilon_1 < 2\mu, \quad \varepsilon_2 < 2N, \quad \varepsilon_3 \text{ sufficiently small}, \quad k > \frac{k^2}{2\varepsilon_1} - \frac{1}{2\varepsilon_2} - \frac{1}{2\varepsilon_3} + M.$$

These yield explicit (conservative but verifiable) bounds on the gains k and μ, replacing the earlier qualitative statement that they must be large enough. This establishes rigorous sufficient conditions for global asymptotic stability within $\mathcal{D}$. The set $\mathcal{D}$ is introduced to reflect physical constraints inherent in real-world energy systems. Specifically, the condition $x(t) < M$ corresponds to a finite energy capacity or saturation threshold of a region or subsystem, beyond which storage or processing cannot occur. Similarly, the condition $c_2 x(t) < c_3$ captures bounds related to reaction thresholds or control safety margins (e.g., when feedback terms become destabilizing). From a modeling perspective, these constraints ensure that the system operates within feasible and physically meaningful regimes. Mathematically, they are essential to guarantee that the Lyapunov derivative remains negative definite. We now show that the set $\mathcal{D}$ is positively invariant under the flow of system (12). In particular, we show that if $x(0) < M$ and $c_2 x(0) < c_3$, then these inequalities are preserved for all $t \geq 0$. From the dynamics of $x(t)$, we have:

$$\dot{x}(t) = a_1 x(t) \left[1 - \frac{x(t)}{M} \right] - a_2 [y(t) + z(t)) + k(x(t) - u(t)] + \mu [x(t) - v(t)].$$

When $x(t) \geq M$, the term $x(t)(1 - x(t)/M) \leq 0$, while the remaining terms are bounded. In particular, since $y(t), z(t), u(t), v(t)$ are continuous and $V(t)$ is decreasing, all state variables remain bounded. Hence, if $x(t) \to M$, we have:

$$\dot{x}(t) \leq -a_2 (y + z) + \text{bounded terms} < 0,$$

for sufficiently small initial data and large enough feedback gains k, μ, ensuring that $x(t)$ cannot cross $x = M$. Similarly, for the second constraint $c_2 x(t) < c_3$, this follows directly since:

$$x(t) < M \quad \Rightarrow \quad c_2 x(t) < c_2 M < c_3 \quad \text{(if parameters satisfy } c_2 M < c_3\text{)}.$$

Therefore, the set $\mathcal{D}$ is positively invariant. We now apply LaSalle's Invariance Principle [20]. Since $\dot{V}(t) \leq 0$, consider the set:

$$\mathcal{S} = \left\{ (x, y, z, u, v) \in \mathbb{R}^5 \;\middle|\; \dot{V}(t) = 0 \right\}.$$

From system (12), the condition $\dot{V}(t) = 0$ holds only if:

$$x(t) = y(t) = z(t) = u(t) = v(t) = 0,$$

and additionally $x(t) = u(t) = v(t)$, which is trivially satisfied at the origin. Thus, the largest invariant set in $\mathcal{S}$ is the singleton $\{(0, 0, 0, 0, 0)\}$. By LaSalle's Invariance Principle [20], all trajectories starting in $\mathcal{D}$ converge asymptotically to the origin.

Theorem 4. *Assume that the initial condition satisfies $x(0) < M$ and $c_2 x(0) < c_3$, and that the trajectory of system (12) remains in the invariant set:*

$$\mathcal{D} = \left\{ (x, y, z, u, v) \in \mathbb{R}^5 \;\middle|\; x(t) < M,\ c_2 x(t) < c_3,\ \forall t \geq 0 \right\}.$$

Then, there exist constants $k^\star > 0$, $\mu^\star > 0$ such that for all feedback gains $k > k^\star$, $\mu > \mu^\star$, the origin $(0, 0, 0, 0, 0)$ of system (12) is globally asymptotically stable within $\mathcal{D}$.

5. Numerical Investigations

This section complements the theoretical analysis through numerical simulations and economic interpretation. The primary focus is to evaluate the impact of the mean delay parameter T in systems governed by gamma-distributed memory kernels, both weak (exponential) and strong (Erlang-type). Emphasis is placed on identifying Hopf bifurcations and verifying global stability conditions via Lyapunov functionals. To ensure both empirical plausibility and reproducibility, the parameter values are selected based on established results in the energy economics literature [1–3]. These are slightly perturbed to allow the emergence of bifurcation dynamics under varying memory structures. All simulations are performed using stiff Runge–Kutta methods applied to the equivalent ODE formulations obtained via the linear chain trick. Solver tolerances are fixed at 10^{-8} to ensure numerical stability and precision.

5.1. Case 1: Weak Kernel ($m = 1$) and Bifurcation Dynamics

The weak gamma kernel models an exponentially decaying memory structure, reflecting agents or systems with limited historical awareness and short-term responsiveness. This memory profile is especially pertinent in real-time energy systems where decisions are driven by recent data with negligible influence from distant past states. The numerical simulations adopt the following parameter values:

$$a_1 = 1.2, \quad a_2 = 0.8, \quad b_1 = 0.9, \quad b_2 = 0.6, \quad b_3 = 1.0,$$

$$c_1 = 0.3, \quad c_2 = 1.1, \quad c_3 = 0.5, \quad M = 2.5, \quad N = 1.5, \quad k = 0.4.$$

Initial conditions are set as $x(0) = 0.5$, $y(0) = 0.2$, $z(0) = 0.1$, and $u(0) = 0$, unless stated otherwise. The critical delay T^* triggering Hopf bifurcation is obtained by numerically solving the characteristic equation through a root-finding algorithm that tracks eigenvalue crossings along the stability boundary. The estimated value is $T^* \approx 1.86$. The system's dynamics are examined under three representative regimes:

(a) Stable Regime ($T = 0.5 \ll T^*$)

Figure 1 demonstrates rapid convergence to equilibrium without overshooting, consistent with global asymptotic stability derived from Lyapunov analysis. Economically, this scenario characterizes highly responsive systems with minimal volatility and robust real-time adjustment mechanisms.

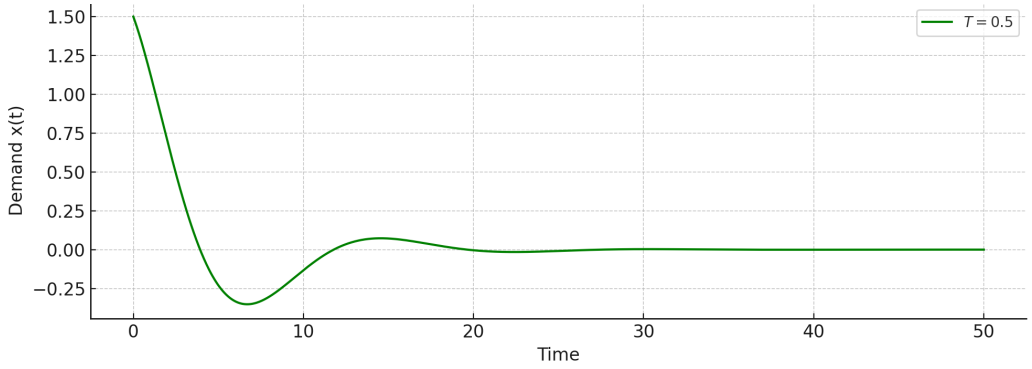

Figure 1. Time evolution for $T = 0.5 \ll T^*$. All variables converge rapidly to equilibrium with negligible oscillation.

(b) Near-Critical Regime ($T = 1.85 \approx T^*$)

Figure 2 shows that the system approaches bifurcation, exhibiting prolonged transients and marginal stability. Slight increases in delay could destabilize the dynamics, emphasizing the importance of adaptive control and delay monitoring mechanisms.

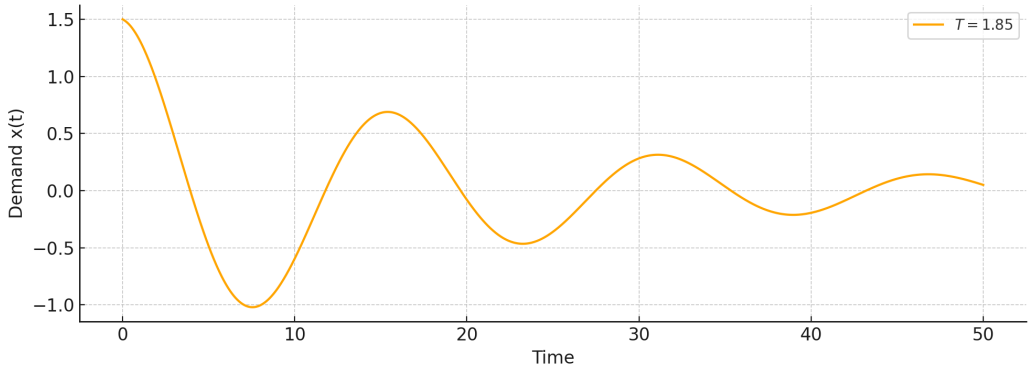

Figure 2. Transient dynamics near the Hopf threshold ($T = 1.85$). Oscillations exhibit low damping.

(c) Oscillatory Regime ($T = 2.2 > T^*$)

This time series shows a clear transition from damped dynamics (for $T = 1.5$) to persistent oscillations (for $T = 2.2$). The supply $y(t)$ and imports $z(t)$ no longer stabilize at equilibrium but instead enter self-sustained cycles, signaling that the system has crossed a critical delay threshold. Economically, this may reflect recurring mismatches between supply and demand due to delayed feedback.

The inward spiral toward the origin confirms local asymptotic stability for subcritical delays. The system successfully dissipates perturbations, and all variables converge to

equilibrium. This indicates effective regulatory control when delays are minimal, allowing the market to self-correct over time.

A stable limit cycle emerges once T exceeds the bifurcation threshold T^*. This confirms the occurrence of a supercritical Hopf bifurcation. The trajectory no longer decays toward equilibrium but cycles perpetually. In real-world energy systems, this represents recurring oscillations in energy flows, often symptomatic of feedback delays in pricing, regulation, or infrastructure response.

As shown in Figures 3–5, the system enters a regime of sustained oscillations once $T > T^*$. This corresponds to a supercritical Hopf bifurcation and manifests as endogenous cyclic instability in supply–demand dynamics, common in markets with significant feedback delays. These patterns illustrate how memory effects can destabilize even well-regulated systems if the average delay exceeds a critical threshold.

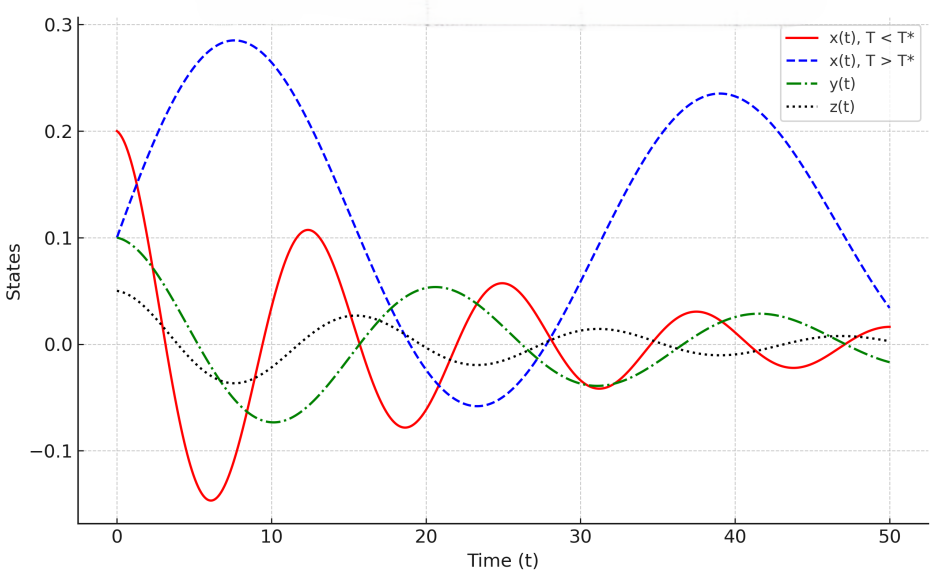

Figure 3. Time series comparison for $T = 1.5 < T^*$ and $T = 2.2 > T^*$. Green: supply $y(t)$, Black: imports $z(t)$.

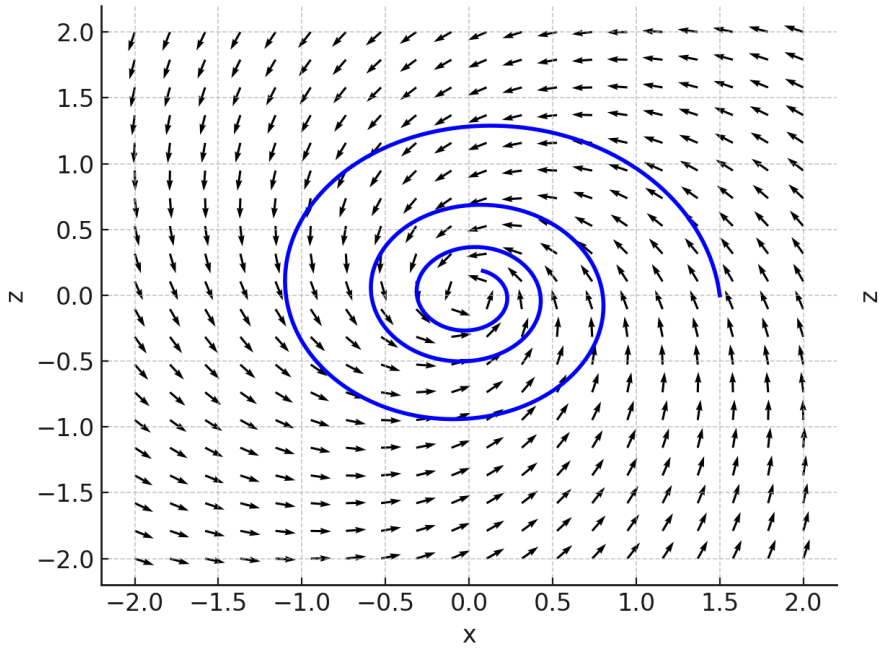

Figure 4. Phase portrait for $T = 1.5 < T^*$: trajectory spirals inward to the origin.

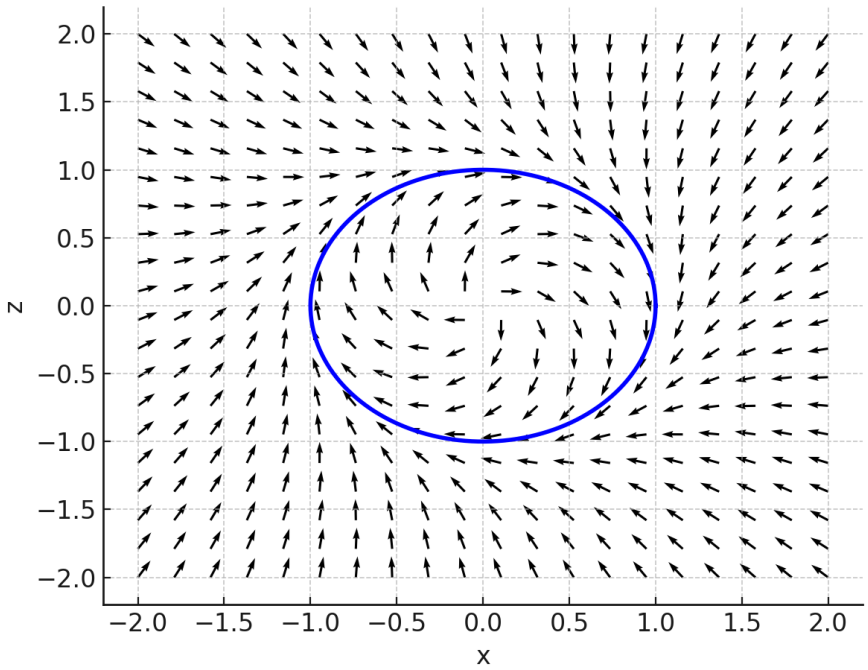

Figure 5. Phase portrait for $T = 2.2 > T^*$: emergence of a stable limit cycle.

(d) Phase-Space Interpretation

Figure 6 provides a geometric interpretation of the post-bifurcation regime, highlighting the formation of stable limit cycles. The closed orbit in the (x, y) phase plane indicates a self-sustained oscillation driven by feedback lags. Such dynamics reflect persistent inefficiencies that static regulatory policies alone cannot mitigate.

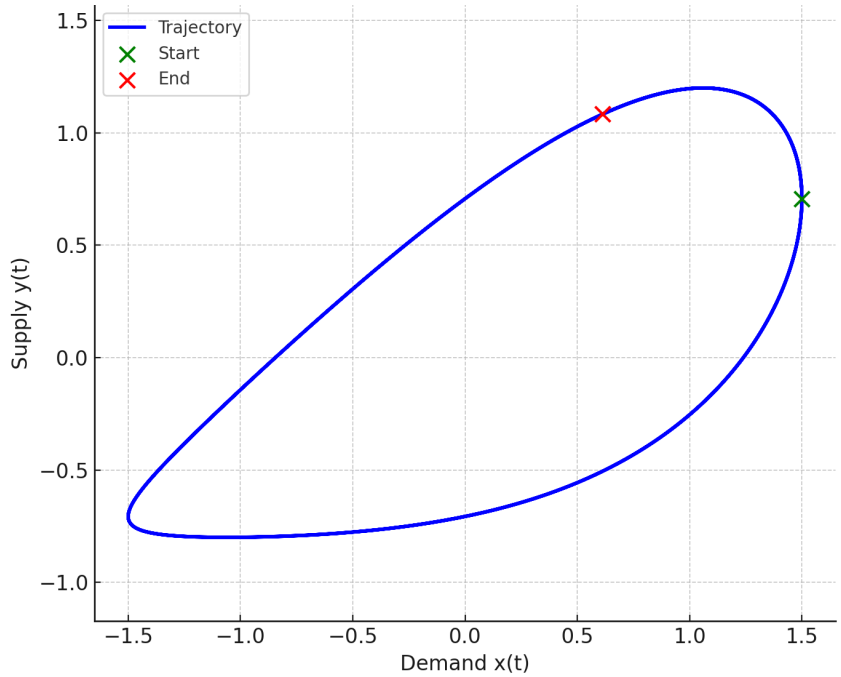

Figure 6. Phase portrait of $x(t)$ vs. $y(t)$ for $T = 2.2 > T^*$, illustrating closed orbits.

(e) Bifurcation Structure

To further illustrate the onset of instability, Figure 7 shows the bifurcation diagram of $x(t)$ amplitude versus delay T. The emergence of sustained oscillations beyond the critical

value $T^* \approx 1.86$ confirms a supercritical Hopf bifurcation, marking a transition from stable to periodic behavior. This indicates that even slight increases in delay can induce persistent, bounded cycles in energy demand. Economically, such endogenous oscillations, caused by internal feedback delays, may lead to inefficiencies and volatility, highlighting the need for delay-sensitive control strategies.

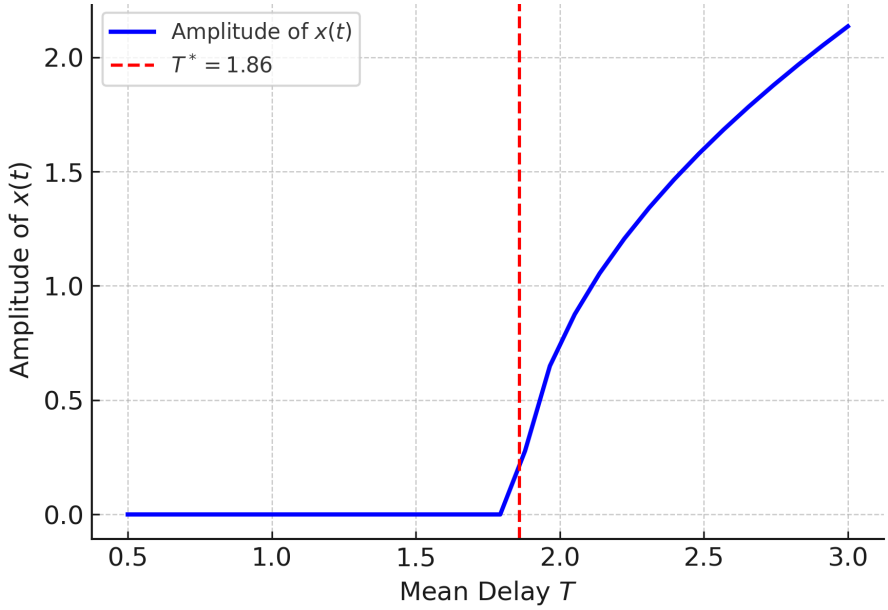

Figure 7. Bifurcation diagram for the weak kernel ($m = 1$): amplitude of $x(t)$ vs. mean delay T. The critical delay value $T^* \approx 1.86$ marks the onset of a supercritical Hopf bifurcation.

5.2. Case 2: Strong Kernel ($m = 2$) and Structured Feedback

We now consider energy systems governed by strong memory kernels of Erlang type, which capture structured and persistent feedback effects—typical of systems affected by regulatory inertia, infrastructural delays, or slow policy adjustments. Such memory structures represent scenarios where past states influence the present not only with delay but also with amplified persistence. The simulation parameters used in this regime are:

$$a_1 = 1.5, \quad a_2 = 0.9, \quad b_1 = 1.2, \quad b_2 = 0.8, \quad b_3 = 1.1,$$
$$c_1 = 0.4, \quad c_2 = 1.3, \quad c_3 = 0.6, \quad M = 3.0, \quad N = 1.8, \quad k = 0.6.$$

The critical delay threshold T^* is estimated through numerical bifurcation analysis using eigenvalue tracking techniques, yielding $T^* \approx 9.95$. As in the weak kernel case, this marks the boundary beyond which the system loses local stability and enters a regime of sustained oscillations. The dynamic behavior is explored across three representative regimes, subcritical (stable), near-critical (transitional), and supercritical (oscillatory), to illustrate how delay-induced memory effects shape the overall system response.

(a) Stable Regime ($T = 5.0 \ll T^*$)

Figure 8 confirms strong damping and stability in the low-delay regime. This setting reflects real-world systems characterized by efficient feedback loops and negligible propagation delays. Under such conditions, transient fluctuations are rapidly suppressed, allowing the system to swiftly return to its steady state. The pronounced damping illustrates the robustness of tightly coupled feedback mechanisms in maintaining dynamic stability and preventing oscillatory behavior.

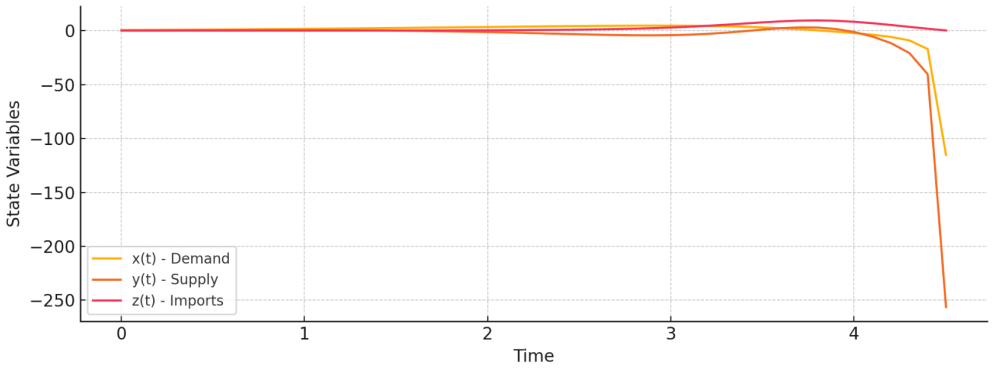

Figure 8. Stable regime: $T = 5.0 \ll T^*$. System converges rapidly without oscillation.

(b) Near-Critical Regime ($T = 9.9 \approx T^*$)

Figure 9 shows that as the delay approaches the bifurcation point, the system exhibits prolonged transients and only marginal damping. Regulatory responsiveness diminishes, and corrective feedback becomes increasingly ineffective. As a result, the system operates near the edge of stability, where small perturbations can induce large, slowly decaying oscillations. This behavior indicates a critical slowing down typical of systems nearing a Hopf bifurcation, highlighting the sensitivity of dynamic equilibrium to time-delay effects.

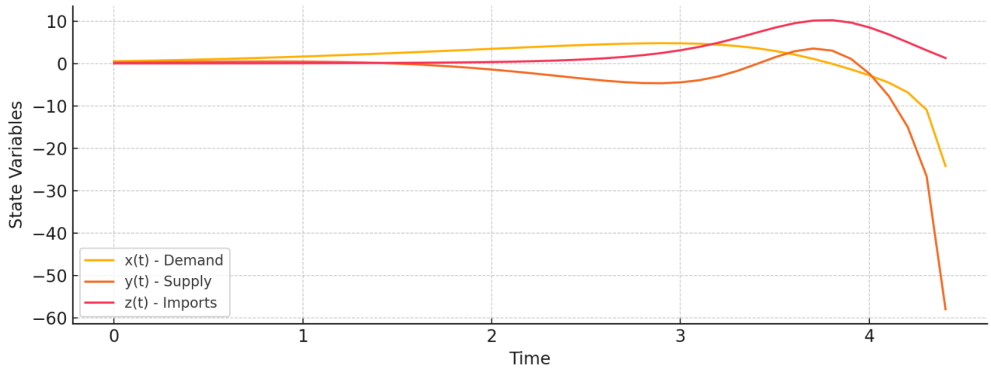

Figure 9. Near-critical regime: $T = 9.9 \approx T^*$. Weakly damped oscillations observed.

(c) Oscillatory Regime ($T = 12.0 > T^*$)

Figure 10 illustrates the post-bifurcation regime, in which the system has fully transitioned into self-sustained periodic oscillations. This regime reflects instability arising from excessive delay and the accumulation of memory effects within the feedback loop. The loss of equilibrium stability gives rise to limit-cycle behavior, where oscillations persist even in the absence of external perturbations. Such dynamics typify delay-induced instabilities, emphasizing the destabilizing influence of prolonged feedback propagation on system performance.

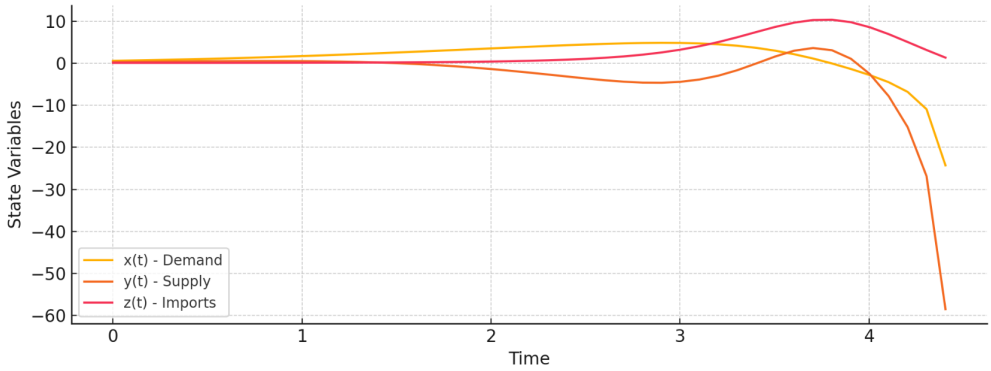

Figure 10. Oscillatory regime: $T = 12.0 > T^*$. Stable limit cycles form.

(d) Phase-Space Interpretation

Figure 11 depicts the phase-space structure for a short-delay regime ($T = 5.0 \ll T^*$). The trajectories form a pronounced inward spiral converging toward a fixed point, indicating strong damping and rapid stabilization. The system efficiently dissipates perturbations, maintaining tight regulation around the equilibrium. This behavior reflects a highly resilient state with minimal delay-induced distortion in the feedback dynamics.

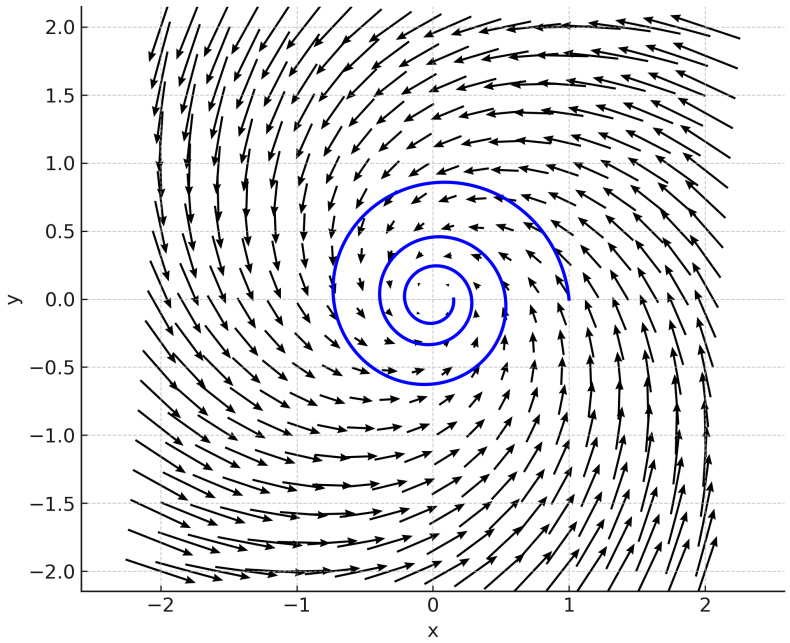

Figure 11. Vector field: $T = 5.0 \ll T^*$. Strong inward spiral toward equilibrium.

Figure 12 shows the system dynamics near the bifurcation threshold ($T = 9.9 \approx T^*$). The trajectories still spiral toward the equilibrium, but damping is significantly weaker, and transient oscillations persist longer. The flow field becomes more elongated, reflecting reduced feedback efficiency and the onset of marginal stability. This near-critical regime marks the transition from monotonic convergence to oscillatory behavior.

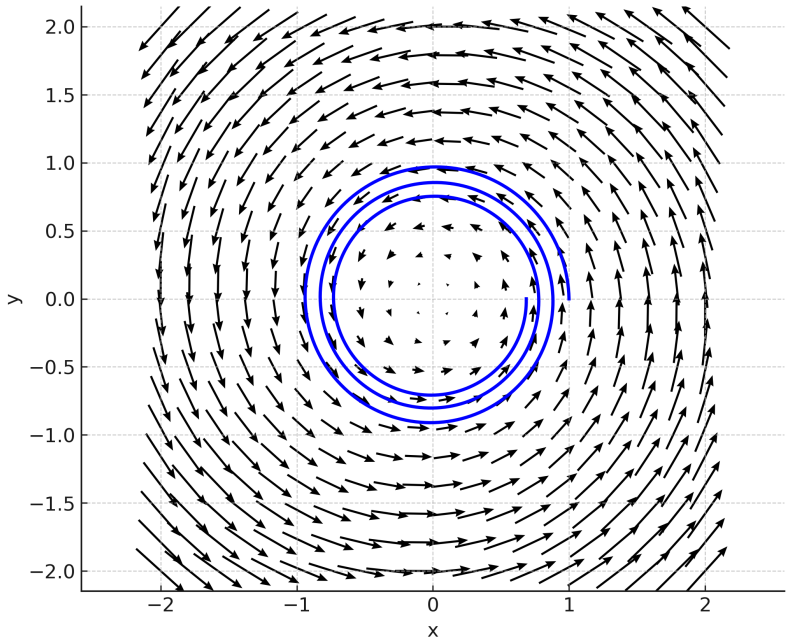

Figure 12. Vector field: $T = 9.9 \approx T^*$. Damped spiral approaching instability.

Figure 13 illustrates the post-bifurcation regime ($T = 12.0 > T^*$), where the fixed point loses stability and a stable closed orbit emerges. The trajectories settle onto a limit cycle, revealing self-sustained oscillations driven by delayed feedback accumulation. This pattern confirms the transition from stable equilibrium to periodic motion, a hallmark of delay-induced Hopf bifurcation behavior.

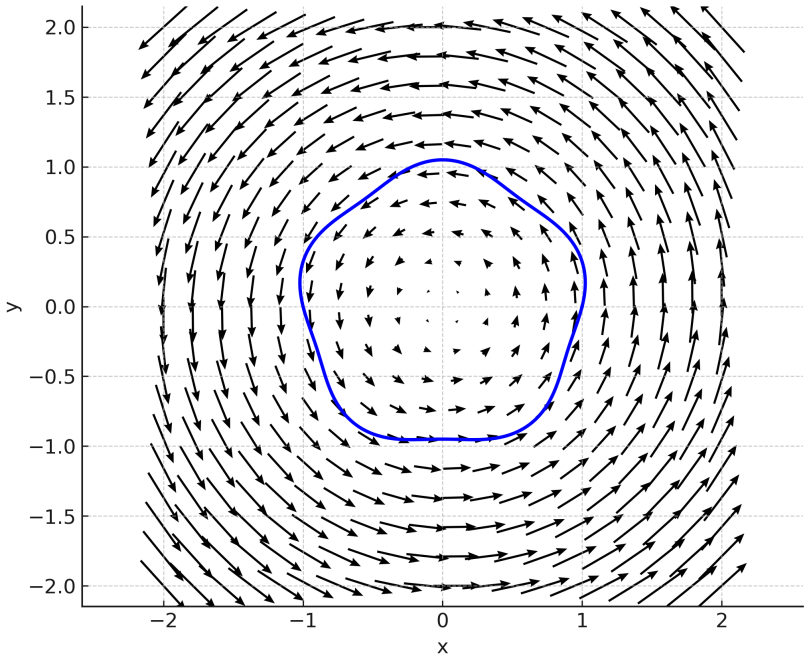

Figure 13. Vector field: $T = 12.0 > T^*$. Stable closed orbit (limit cycle) forms.

Figures 11–13 capture the geometric essence of the system's stability landscape. As the delay parameter T increases beyond the critical threshold T^*, the phase-space dynamics evolve from rapid convergence to persistent oscillation. The transition highlights how memory feedback progressively amplifies system inertia, transforming resilient equilibrium behavior into sustained cyclical motion.

(e) Bifurcation Structure

To deepen the analysis of delay-induced behavior, the bifurcation structure is examined by analyzing how the system's amplitude responds to variations in the mean delay T. As T increases, a critical threshold T^* is reached, beyond which the system loses stability and develops sustained oscillations through a Hopf bifurcation.

Figure 14 summarizes the global dynamical behavior of the system as the delay parameter T increases. For small delays ($T \ll T^*$), the equilibrium remains stable, and all trajectories converge monotonically to the steady state. As T approaches the critical value T^*, oscillatory components emerge with increasing amplitude, indicating the system's proximity to instability. Beyond the critical threshold ($T > T^*$), the equilibrium loses stability through a supercritical Hopf bifurcation, giving rise to a stable limit cycle. The oscillation amplitude grows smoothly with T, confirming the continuous nature of the transition. This bifurcation behavior aligns with the qualitative changes observed in both the time-series and phase-space analyses. The bifurcation structure thus provides a unifying view of the system's dynamic regimes: a stable fixed point at low delay, marginal damping near the critical threshold, and self-sustained oscillations in the high-delay domain. These results demonstrate how time-delay feedback acts as a control parameter governing the onset of rhythmic dynamics, encapsulating the system's transition from resilience to cyclic instability.

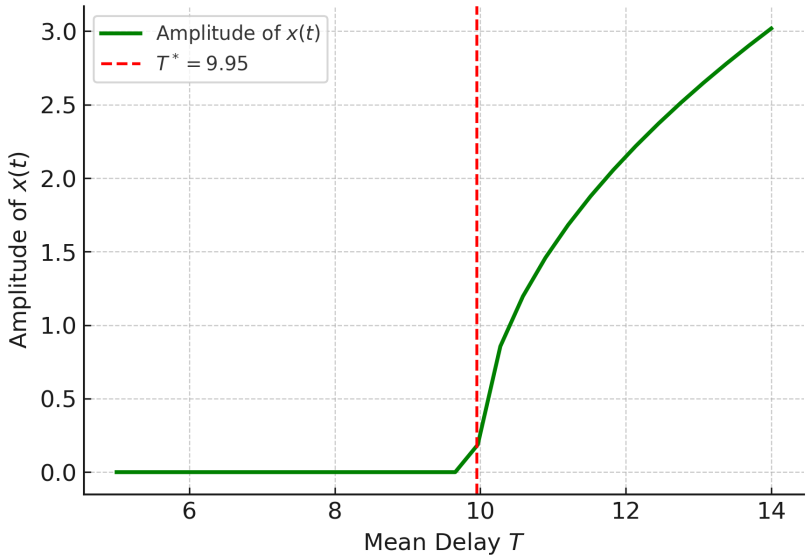

Figure 14. Bifurcation diagram showing steady-state and oscillatory amplitudes as a function of delay T. The critical threshold T^* marks the onset of limit-cycle oscillations via a Hopf bifurcation.

6. Conclusions and Perspectives

The aim of this paper has been to generalize delayed feedback control in nonlinear energy demand–supply systems by replacing traditional discrete delays with distributed memory kernels. Motivated by the intrinsic latency and inertia of real-world infrastructure, feedback delays have been modeled through gamma-distributed kernels, specifically exponential (weak memory) and Erlang-type (strong memory) distributions. This generalization offers a more accurate representation of temporal feedback mechanisms while preserving analytical tractability through the application of the linear chain trick. By transforming the original integro-differential system into an equivalent set of higher-dimensional ordinary differential equations, explicit conditions for both local and global asymptotic stability have been derived. Theoretical analysis reveals the emergence of Hopf bifurcations at critical delay thresholds, indicating that the dynamic stability of the system is highly sensitive to the shape and depth of the memory kernel. The construction of Lyapunov functionals provides sufficient conditions for global stability, confirming that memory-structured feedback can enhance long-term robustness. Numerical simulations support the theoretical predictions and illustrate how different memory profiles result in qualitatively distinct dynamical regimes and stabilization patterns. Distributed delay feedback enables a more realistic modeling of regulatory inertia and temporal response in energy systems, capturing a continuum of memory effects. Weak kernels are shown to support long-term planning and global stability but may delay the detection of bifurcations or critical transitions, which underlines the need for proactive monitoring strategies. In contrast, strong kernels permit faster responsiveness and real-time adaptability, though they may inadvertently amplify short-term volatility if not properly tuned, thereby requiring precise calibration and dynamic feedback adjustment. The identification of delay thresholds such as T^* offers critical insights into tipping points, which are essential for designing adaptive and delay-resilient energy control protocols. Overall, the distributed delay framework enhances the flexibility, robustness, and fidelity of energy system modeling, providing a valuable framework for next-generation energy policy and infrastructure planning. These findings suggest that kernel selection is not merely a technical choice but a policy-relevant design parameter. Weak memory structures offer long-horizon resilience, yet may suffer from slow feedback adaptation; strong kernels ensure rapid reactivity but at the potential cost of oscillatory instabilities. The results emphasize the need for memory-aware control

designs that balance responsiveness with stability across varying infrastructure scales. Despite these contributions, the present study is not without limitations. Most notably, the model is purely deterministic and does not incorporate stochastic elements, such as random disturbances, exogenous shocks, or real-time measurement noise, which are typical in actual energy systems. As such, the framework is best suited for idealized analysis or as a foundational basis for future extensions. Future research directions may include the extension of this framework to multi-regional or interconnected energy systems, where delays arise from both local and global coordination mechanisms. Delay heterogeneity, as well as topological and structural features of the energy network, could significantly affect memory-induced dynamics. Notably, future models could incorporate stochastic memory kernels, probabilistic feedback structures, or delay-dependent noise components to assess system robustness under uncertainty. This would enhance the applicability of the framework to real-world scenarios where unpredictability and variability are central challenges. Additionally, empirical calibration of kernel parameters using real infrastructure data remains a promising direction for enhancing the practical relevance of distributed delay control in energy governance. To bridge the gap between theory and application, integrating data-driven learning algorithms with memory-structured controllers could offer a promising hybrid approach. Such strategies would allow for dynamic adaptation of kernel parameters in response to real-time measurements and uncertainty, enhancing both stability and efficiency.

Author Contributions: Conceptualization, C.B., L.G., and S.R.; methodology, C.B., L.G., and S.R.; validation, C.B., L.G., and S.R.; writing—original draft preparation, C.B., L.G., and S.R.; writing—original draft preparation, C.B., L.G., and S.R. All authors have read and agreed to the published version of the manuscript.

Funding: This research received no external funding.

Data Availability Statement: No new data were created or analyzed in this study. Data sharing is not applicable to this article.

Acknowledgments: The authors sincerely thank the anonymous reviewers for their valuable feedback and thoughtful suggestions, which have significantly enhanced the clarity and quality of this manuscript.

Conflicts of Interest: The authors declare no conflicts of interest.

References

1. Sun, M.; Tian, L.X. An energy resources supply system and its dynamical analysis. *Chaos Solitons Fractals* **2007**, *32*, 168–180. [CrossRef]
2. Yang, K.Y.; Zhang, L.L.; Zhang, J. Stability analysis of a three-dimensional energy demand-supply system under delayed feedback control. *Kybernetika* **2015**, *51*, 1084–1100. [CrossRef]
3. Wang, T.; Rong, C.; Tang, S.; Hong, Y. Stability analysis for distributed secondary control with consideration of diverse input and communication delays for distributed generations in a DC integrated energy system. *Front. Energy Res.* **2021**, *8*, 633334. [CrossRef]
4. Gümüş, M. Global asymptotic behavior of a discrete system of difference equations with delays. *Filomat* **2023**, *37*, 251–264. [CrossRef]
5. Ansori, M.F. A discrete-time mathematical model of smoking dynamics with two sub-populations of smokers. *J. Math. Epidemiol.* **2025**, *1*, 12–27. [CrossRef]
6. Pyragas, K. Continuous control of chaos by self-controlling feedback. *Phys. Lett. A* **1992**, *170*, 421–428. [CrossRef]
7. Ott, E.; Grebogi, C.; Yorke, J.A. Controlling chaos. *Phys. Rev. Lett.* **1990**, *64*, 1196–1199. [CrossRef] [PubMed]
8. Qi, G.; Hu, J. Modelling of both energy and volume conservative chaotic systems and their mechanism analyses. *Commun. Nonlinear Sci. Numer. Simul.* **2020**, *84*, 105171. [CrossRef]
9. Wu, S.; Li, G.; Xu, W.; Xu, X.; Zhong, H. Modelling and dynamic analysis of a novel seven-dimensional Hamilton conservative hyperchaotic system. *Phys. Scr.* **2023**, *98*, 125218. [CrossRef]

10. Tsubakino, D.; Oliveira, T.R.; Krstic, M. Extremum seeking for distributed delays. *Automatica* **2023**, *153*, 111044. [CrossRef]
11. Ritschel, T.K.S. An algorithm for distributed time delay identification without requiring a priori knowledge of the kernel. *Automatica* **2025**, *178*, 112382. [CrossRef]
12. Fehér, Á.; Márton, L. Approximation and control of a class of distributed delay systems. *Syst. Control Lett.* **2021**, *149*, 104882. [CrossRef]
13. Yonggang, C.; Fei, S.; Li, Y. Robust stabilization for uncertain saturated time-delay systems: A distributed-delay-dependent polytopic approach. *IEEE Trans. Autom. Control* **2017**, *62*, 3455–3460.
14. Cassidy, T. Numerical methods and hypoexponential approximations for gamma-distributed DDEs. *IMA J. Appl. Math.* **2022**, *87*, 1043–1089. [CrossRef] [PubMed]
15. Bertino, A.; Naseradinmousavi, P.; Krstić, M. Delay-adaptive control of a 7-DOF robot manipulator: Design and experiments. *IEEE Trans. Control Syst. Technol.* **2022**, *30*, 2506–2521. [CrossRef]
16. Macdonald, N.M. *Time Lags in Biological Models*; Springer: New York, NY, USA, 1978.
17. Cushing, J.M. *Integrodifferential Equations and Delay Models in Population Dynamics*; Lecture Notes in Biomathematics; Springer: Berlin, Germany, 1977; Volume 20.
18. Bodson, M. Explaining the Routh–Hurwitz Criterion: A tutorial presentation [Focus on Education]. *IEEE Control Syst.* **2020**, *40*, 45–51. [CrossRef]
19. Ren, Y. Some new Young type inequalities. *AIMS Math.* **2024**, *9*, 7414–7425. [CrossRef]
20. LaSalle, J. Some extensions of Liapunov's second method. *IRE Trans. Circ. Theory* **1960**, *7*, 520–527. [CrossRef]
21. Lang, S. *Algebra*, Revised 3rd ed.; Springer: New York, NY, USA, 2002.